Earthquake scaling, fault segmentation, and structural maturity

Isabelle Manighetti *, Michel Campillo, Sylvain Bouley, Fabrice Cotton

Laboratoire de Géophysique Interne et Tectonophysique de Grenoble, Grenoble, France

Abstract

Slip and length measurements on earthquakes suggest large stress drop variability. We analyze an extended set of slip-length measurements for large earthquakes ($M \geq 6$) to seek for the possible origin(s) of this apparent variability. We propose that such variability arises from earthquakes breaking a variable number of major fault segments. That number depends on the strength of the inter-segment zones, which itself depends on the structural maturity of the faults. We propose new D_{max}–L parameterizations based on that idea of multiple segment-ruptures. In such parameterizations, each broken segment roughly scales as a crack, while the total multi-segment rupture does not. Stress drop on individual segments is roughly constant, only varying between 3.5 to 9 MPa. The slight variation that is still observed depends on fault structural maturity; more mature faults have lower stress drops than immature ones. The new D_{max}–L functions that we propose reduce uncertainties with respect to available relationships. They thus provide a more solid basis to estimate seismic hazard by integrating fault properties revealed by geological studies.
© 2006 Elsevier B.V. All rights reserved.

Keywords: Earthquakes osin; Scaling; Slip-length; Fault maturity; Fault segmentation

1. Introduction

A common hypothesis in earthquake mechanics is that earthquakes have a macroscopic behavior of cracks in an elastic medium, with the stress drop being a material property hence being almost constant for crustal earthquakes e.g., [1–5]. From that hypothesis, one expects maximum (D_{max}) or mean displacement (D_{mean}) on earthquakes to scale with rupture length (L) when $L \leq 2W_{seism}$ (W_{seism} being the thickness of the seismogenic layer), and tapers off for long ruptures ($L > 2W_{seism}$). While available D–L earthquake data have long been too few to show whether or not that

behavior was real (see stormy debate that opposed 'L- and W-model' supporters over 15 yr; [6–12]), it is now generally admitted (exceptions are [13,14]), from examination of denser data sets, that earthquakes more likely follow a 'W-model', hence roughly behave as cracks [15–17]. Shaw and Scholz (2001; later referred to as S&S01) have recently proposed a scale-invariant physical model that includes the two D–L regimes:

- for ruptures with $L \leq 2W$, $D_{mean} = \alpha * (L/2)$
- for ruptures with $L > 2W$, $D_{mean} = \alpha * (1/[1/L + 1/2W])$ (1)

It is important to note that, in the formulation of that equation, S&S01 postulate that α is proportional to a constant static stress drop, while W represents the width

* Corresponding author.
  E-mail address: imanighe@obs.ujf-grenoble.fr (I. Manighetti).

of the seismogenic layer thus is W_{seism}. The model roughly reproduces the first-order distribution pattern of ∼55 earthquake slip-length data (see their Fig. 1). While this suggests that the physical basis of the model is appropriate overall, a closer examination of the data suggests that an additional factor may intervene in the D–L scaling for actual D–L data are much more scattered than predicted by the constant stress drop
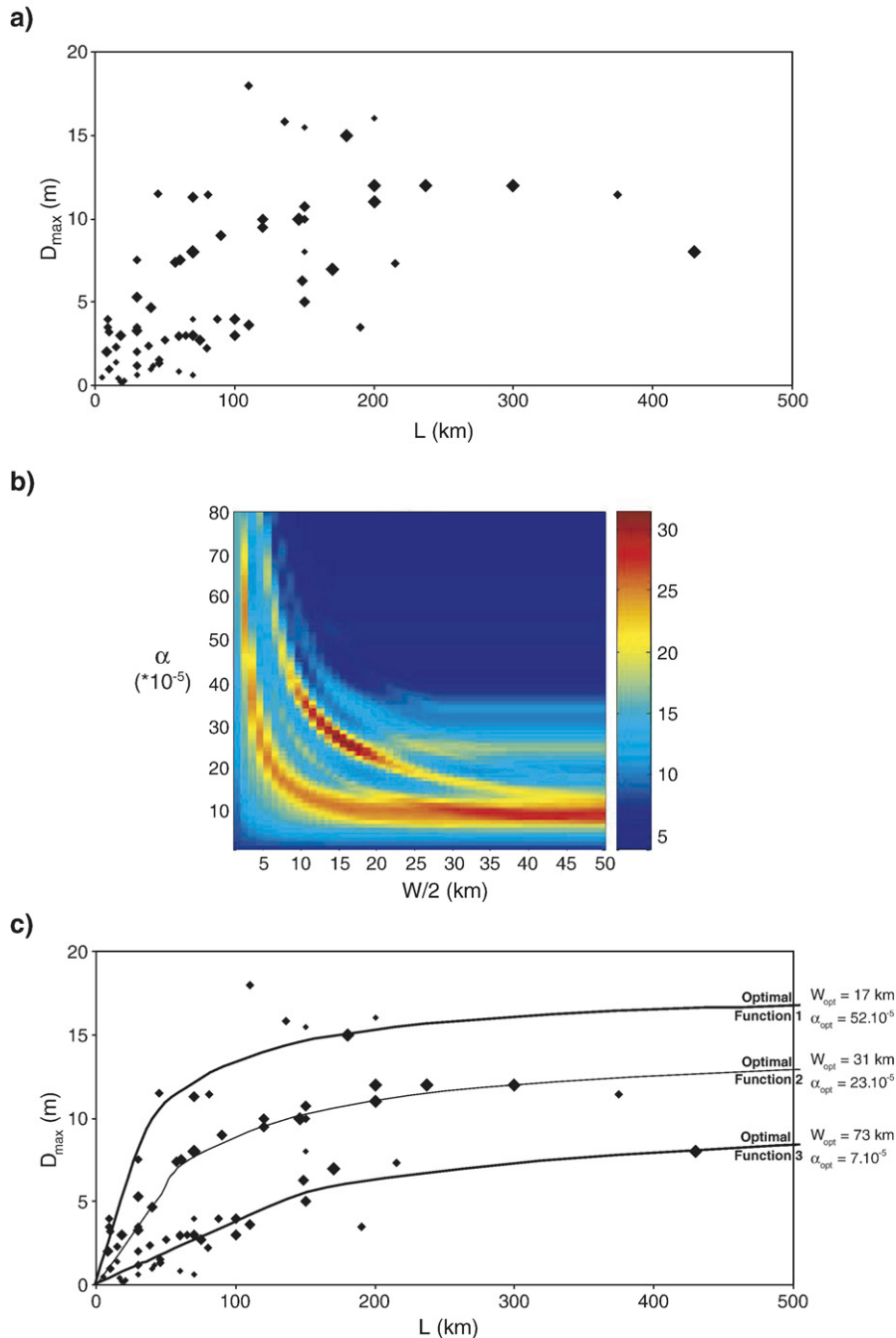

Fig. 1. Displacement-length surface data in Asia (from Table 2). (a) D_{max} versus L plot. Symbol size is proportional to quality weight. (b) Fit quality map resulting from adjusting the data set with one S&S01' function having variable $[\alpha, W]$ values. Three, and possibly fours regions of $[\alpha, W]$ values are found that best-fit distinct data subsets. (c) Data are plotted together with the three optimal S&S01' functions deduced from B. Corresponding optimal $[\alpha, W]$ values are indicated.

model; large earthquakes of similar size (i.e., similar length and width) obviously can produce different slips and stress drops, as it has been pointed out by many authors e.g., [2,17–21]. We focus here on such slip variability and seek for its possible origin(s). We compile all available slip-length measurements for large earthquakes in four seismically active regions of the world. Our data set only includes earthquakes with a magnitude larger than ~6, so that our results are relevant to the largest scale of the earthquake process only. We conduct our analysis using the functional form of Eq. (1). Yet, we give an interpretation of the parameters α and W that is different, though not contradictory, with that of S&S01. We state that the observed slip variability arises from broken geological faults having a variable frictional strength that depends on their long-term slip history ('structural maturity') and geometry (large-scale segmentation). While the effect of slip history has already been evoked in earthquake scaling analyses e.g., [18,22–25], that of fault segmentation has never been. We claim that it should be, for it dictates the way earthquakes gain in length, hence strongly governs the relationship(s) between earthquake slip and length.

2. Data sets

We examine displacement-length data for a set of ~250 large ($M \geq ~6$), shallow (rupture width ≤40 km, with an average value W_{mean} of 18 km), continental earthquakes of mixed focal mechanisms (strike–slip, reverse and normal), that have occurred in four of the most seismically active regions worldwide: Asia (broad sense), Turkey, West US, Japan. In these regions, long-term active faults are generally well known, with their surface geometry (total length, segmentation, strike variations, associated secondary fault networks), age, maximum slip rate and total cumulative displacement being generally determined. We use these long-term parameters (where available) to qualify the structural maturity of the faults that broke during the analyzed earthquakes, as explained in Table 1 (supporting online material). Doing so, we classify the broken faults in three classes, basically 'immature', 'intermediate', and 'mature' (Table 1). Earthquake slip-length data are compiled from literature (references in Tables 2 and 3; supporting online material). We consider here the maximum displacement (D_{max}), not the mean (D_{mean}), for it is best constrained. Besides, Manighetti et al. [21] have shown that $D_{max} = 2 * D_{mean}$ for most large earthquakes worldwide, a property that is found to be scale-independent. Being aware that rupture slip and length measured at surface may be lower than actual maximum

slip and length produced at depth, we compile both surface measurements (209 earthquakes; Table 2) and slip-length values inferred at depth from earthquake source models (56 earthquakes; Table 3), and analyze them separately. Surface data are screened for quality, and a 'quality weight' assigned to each data from criteria defined in Table 2. Note that, since error bars cannot be properly defined for most data, weighting them with a quality factor is the best we can do to discriminate poor and robust data. While such quality screening is a fundamental step to discuss any scaling law, it has never been done before (in terms of quality weighting of each data). Concerning slip-length data at depth, we did not attempt to 'qualify' the quality of the various earthquake source models. Rather we chose to average the different D_{max}–L values proposed for the same earthquakes (Table 3).

3. Data analysis

We start analyzing in detail the Asian data set, for it is the densest. Fig. 1a shows the Asian surface D_{max}–L data, with symbol size proportional to quality weight. The data are rather dispersed, so that a single function cannot be found to adjust them all properly. However the overall shape of the data distribution resembles an asymptotic function similar to that predicted by the S&S01' model; slip increases with length for short ruptures ($L < 100$–200 km), and seems to saturate for longer ruptures. We note that, while data are dispersed, they do not extend evenly over the plot; there are zones free of data, and zones where data cluster. This suggests the existence of a few specific trends. To check whether or not these trends are significant, we use a figure of merit M to score the adjustment of a couple of [α, W] parameters to the data set, and explore the whole space of the model parameters (Fig. 1b). M is of the form $M = \sum_i (ch([D_{obs} - D_{(\alpha,W)}]/D_n))^{-1}$ where D_{obs} is the measured value of slip, $D_{(\alpha,W)}$ is the predicted value of slip, and D_n is an adjustable smoothing parameter (chosen here to be 7 times the standard deviation of D_{obs}). At this stage, we thus assume that α and W are free adjustment parameters. The existence of several, distinct zones of maximum in Fig. 1b indicates that the data cannot be fitted with a single model, but rather include several subsets associated with different models, i.e. different values of [α, W]. Three major zones are identified, whose shape is related to bias between α and W. Since we deal with a limited number of data, we must verify that this multimodal structure is not fictitious. We generated random models having the statistical properties of the data (average and variance of D depending on

L, distribution of L) and performed the same test as before. The multimodal structure with respect to the functional form of S&S01 that is exhibited by the data is not produced by sparse random series. We checked a

dozen realizations to reach this conclusion. Examples are presented in Fig. A (supporting online material). We can thus conclude on firm ground that the Asian surface data set actually includes at least 3 distinct groups
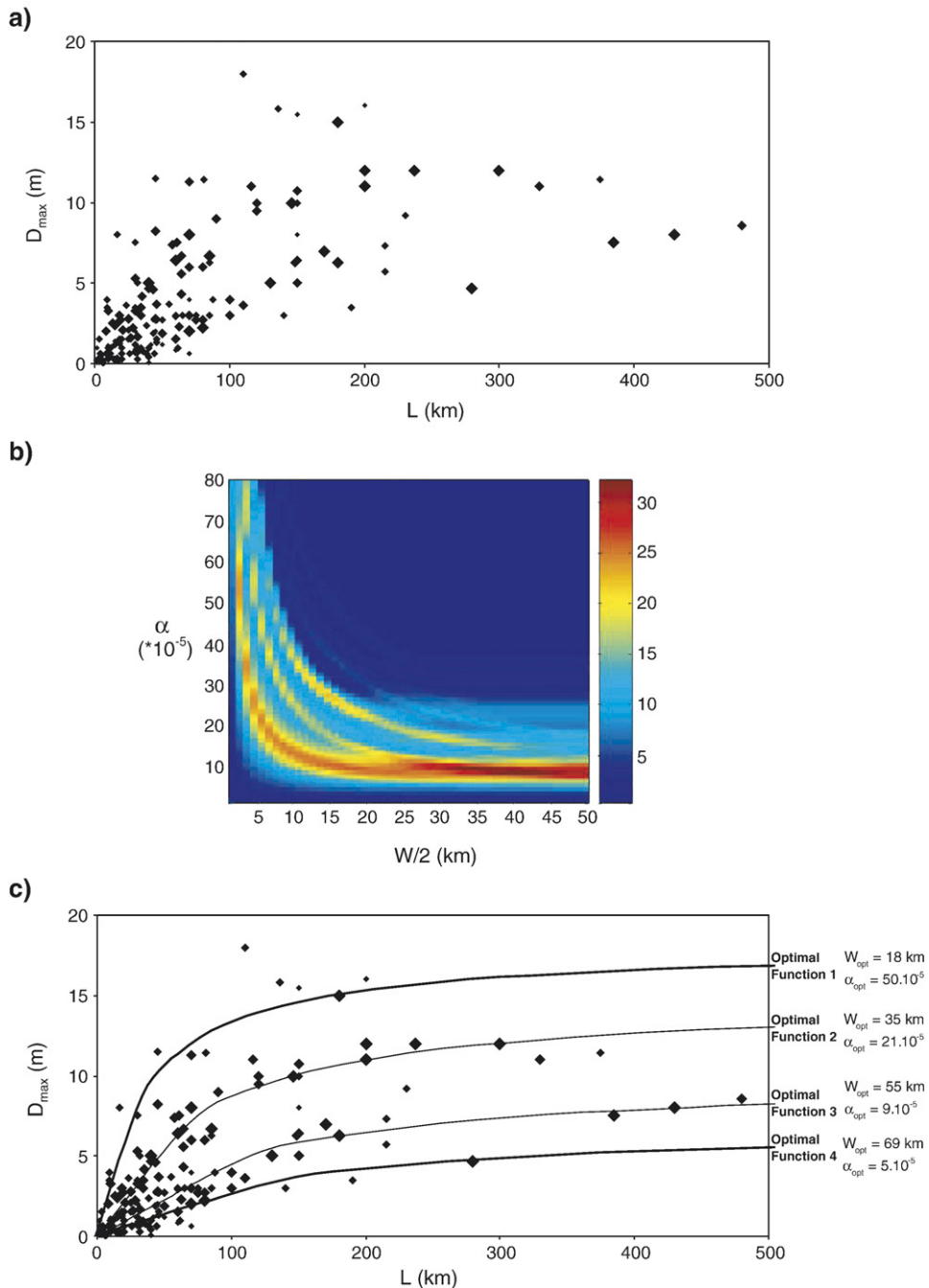

Fig. 2. Displacement-length surface data in the four Asia, West US, Turkey and Japan regions (from Table 2). (a) D_{max} versus L plot. Symbol size is proportional to quality weight. (b) Fit quality map resulting from adjusting the whole data set (smallest ruptures with $L<50$ km are excluded for clarity) with one S&S01' function having variable $[\alpha, W]$ values. Three, and possibly fours regions of $[\alpha, W]$ values are found that best-fit distinct data subsets. (c) Data are plotted together with the four optimal S&S01' functions deduced from b. Corresponding optimal $[\alpha, W]$ values are indicated.

unambiguously associated with different couples of [α, W] parameters. Based on these findings, we searched for the three optimal S&S01' functions that combine to produce the best fit to the entire data set. This is done through an iterative optimization procedure in which each data point is affected to a subset. Fig. 1c shows the results, together with the three couples of optimal [α, W] values best adjusting the data. We find that data are properly fitted provided that W and α both vary. In the last section of the paper, we discuss statistical tests (using Akaike Information Criterion) that show that the misfit reduction is not due to 'over-fitting' the data with models having a too large number of free parameters. The optimal values of W are found to be regularly spaced, the largest being about multiple of the lowest, while α varies irregularly yet decreasing with W. Note that these results are independent of slip mode; strike–slip, reverse and normal ruptures are found in any of the three groups (Fig. B, done for all data; supporting online material).

We applied the same treatment to the other three regional data sets. In all cases the data show a multimodal structure, with at least two or three distinct regions of [α, W] values found to adjust distinct data subsets (Fig. C, supporting online material). Fig. D (supporting online material) shows the corresponding optimal S&S01' functions. In all cases, the optimal [α, W] parameters vary in a discrete, almost regular fashion. Besides, the optimal [α, W] values are roughly similar from one region to the other, so that, on average, 4 recurrent, multiple couple values are suggested, equal to [$(46\pm6).10^{-5}$, 17.5 ± 0.5], [$(20\pm2).10^{-5}$, 32 ± 3], [$(8\pm1).10^{-5}$, 57 ± 4], and [$(5\pm1).10^{-5}$, 71.5 ± 1.5].

Fig. 2a now shows all surface data together. The uneven data distribution appears more clearly, with three main trends distinguishable. Fig. 2b confirms that the whole data set consists of three or four distinguishable data subsets associated with distinct domains of [α, W]. Fig. 2c shows the four optimal S&S01' functions that we inferred from this basis. These functions again suggest
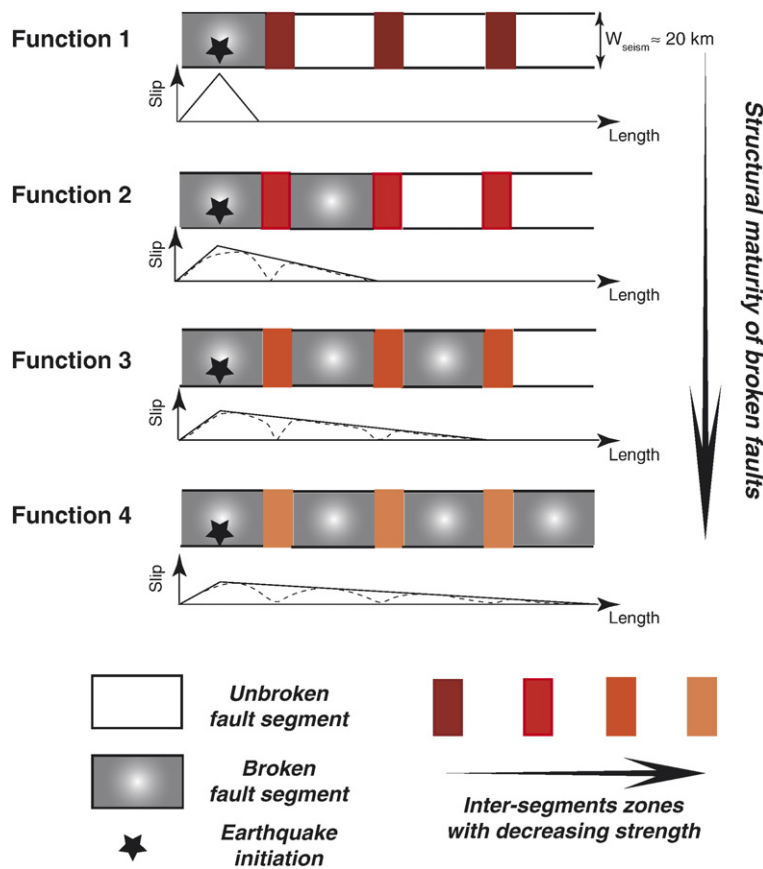

Fig. 3. Proposed scenario. Earthquakes break a variable number of major segments along the faults on which they initiate. That number increases with the degree of structural maturity of the faults, for inter-segments zones have lower strength on mature faults. The shape and amplitude of the resulting slip profiles varies accordingly.

discrete values of W, roughly equivalent to the lowest 18 km value being multiplied by 1 to 4 when one goes from optimal functions 1 to 4. The parameter α is also found to vary in a discrete, yet more irregular fashion.

Finally, Fig. F (supporting online material) shows all slip-length data at depth deduced from inversion models, together with the four optimal S&S01' functions whose existence is inferred, as before, from analysis of Fig. E (supporting online material). Though the data set is different, the optimal W values are similar to those obtained from surface data, while the optimal α values are slightly higher.

Together these results highlight major issues. First, the finding that all data sets contain several distinct data subsets, hence request the combination of several distinct D_{max}–L functions to be adjusted overall, demonstrates that an additional parameter, other than W_{seism} and a constant stress drop, intervenes in the relationship between rupture slip and length (note that this makes that relationship not being strictly speaking a 'scaling law'). Second, the optimal S&S01' functions that are inferred imply variable values of W. Thus, the single crack model does not apply in its simple form. Besides, the range of variation of W is large, while the obtained values are roughly multiple of the lowest. Together these are incompatible with W being the seismogenic thickness. We thus need to admit that W does not represent the width of the seismogenic zone. Rather it is a characteristic length at which slip saturates, to which we will give an interpretation in the following. Finally, the optimal functions that we find also imply variable values of α, thus of stress drop, given by $\Delta\sigma = \mu * (\alpha/2)$ with $\mu = 3.10^{10}$ in the original S&S01 interpretation. For instance, when the stress drop is calculated from the inversion model data (total slip values, Fig. F), these variations appear to be quite large, ranging between ~9 and 1 MPa as one goes from optimal functions 1 to 4. Such large variations are incompatible with the constant stress drop hypothesis. This further confirms that the crack model scaling does not apply to earthquakes in its simple form.

4. Interpretation

This led us to seek for a scenario that would retain basic, reasonable ingredients such as the elastic crack behavior and the reality of the seismogenic thickness (W_{seism} ~ 18 km for our data), while allowing the parameter W in Eq. (1) to take discrete values increasing algebraically. As said before, that fitting parameter W is not W_{seism}, and is unlikely to represent the thickness of anything real for the obtained optimal values do not coincide with any known feature of the Earth structure.

We thus hypothesize that W rather is the half rupture length at which slip starts saturating (L_{sat}); we actually observe that slip starts saturating at different lengths along the analyzed ruptures. Some earthquakes would behave as 'simple cracks', having $L_{sat} = 2W_{seism}$, while some earthquakes would be more complex, with their slip starting to saturate at greater lengths observed to be 2, 3 or 4 times longer than that for a single crack ($L_{sat} = n * (2W_{seism})$ with n between 2 and 4). This behavior suggests that those earthquakes are made of several cracks juxtaposed along the rupture strike. This recalls fault segmentation. Indeed, geological faults are segmented, made of a finite number of large-scale segments [26–29]. Note that we are referring here to the segmentation that affects a fault at its largest scale; not to 'slip heterogeneity' on fault planes as commonly described in seismological literature e.g., [30]. The first-order segments that we are evoking thus are of about the same scale than the whole fault they belong to (at most shorter by one order). Generally, only 3–4 such large-scale segments are identified along a fault, independent of its slip mode e.g., [26,27,29,31,32]. As a fault grows with time, linkage between its large-scale segments evolves from 'soft' (i.e., segments are hardly linked) to 'hard' (i.e., segments are fully linked) e.g., [33–36], so that the geometry of the fault zone simplifies and becomes more continuous, more 'through-going' [26,28,37]; inter-segment zones evolve from being wide areas of distributed, disorganized, secondary fissuring and faulting, to becoming narrow zones of localized, through-going faulting. We thus expect the zones that connect the large-scale segments to have an apparent strength that depends on the structural maturity of the overall fault they belong to; high on young, immature faults, and lower on long-lived, mature features [28,29]. Large-scale inter-segment areas may thus behave as more or less 'resistant barriers' to earthquake rupture 'propagation', as has actually been observed in many cases e.g., [21,38–42]. We propose that, depending on the strength of these inter-segment barriers, an earthquake may eventually break a variable number of large-scale segments along the fault on which it initiates. On mature faults, the breakage of a first segment may easily overcome the resistance of the inter-segment barriers, so that it may trigger the cascading rupture of several segments along the fault, resulting in a long, multi-segment rupture. By contrast, on immature faults, the breakage of a first segment is unlikely to overcome the barriers that disorganized, wide inter-segment zones represent, so that only one segment may eventually break, resulting in a short, crack-like rupture. Fig. 3 shows the scenario that we envision. In that scenario, segments have the same length and width (equal to W_{seism} for large earthquakes), while the size of barriers

is neglected. Segments behave independently, so that each breaks as an elastic crack. Thus, if only one fault segment breaks, slip starts saturating at $L_{sat} = 2W_{seism}$. But if the inter-segment barriers are 'weak enough' to allow cascading triggering, two, three or more segments along the fault may break in succession, leading to increase L_{sat} by as many times as there are broken segments (Fig. 3).
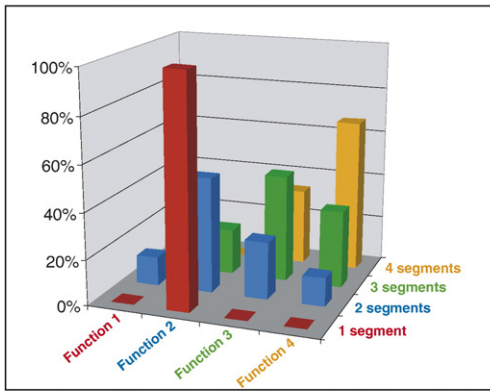
5. Facing the model with independent observations

We now test that hypothesis further. A first test consists in facing the actual number of major fault segments broken during earthquakes to the four optimal functions determined earlier (Fig. 4a). We found such
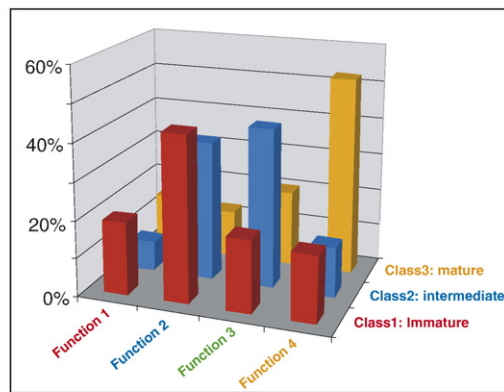
information for ~40 earthquakes (details in Table 2). Fig. 4a shows that, overall, earthquakes that have broken one or two major segments pertain to the data subsets that are best fitted by the optimal functions 1 or 2, while earthquakes that have broken 3 to 4 segments pertain to the data subsets that are best fitted by the optimal functions 3 or 4. This is in keeping with the scenario that we propose (Fig. 3).

Another piece of information comes from Manighetti et al. [21]. These authors have studied the generic properties of earthquake slip profiles and shown that these profiles have a self-similar triangular shape that is roughly symmetric when a single major fault segment has been broken, and asymmetric to a various degree
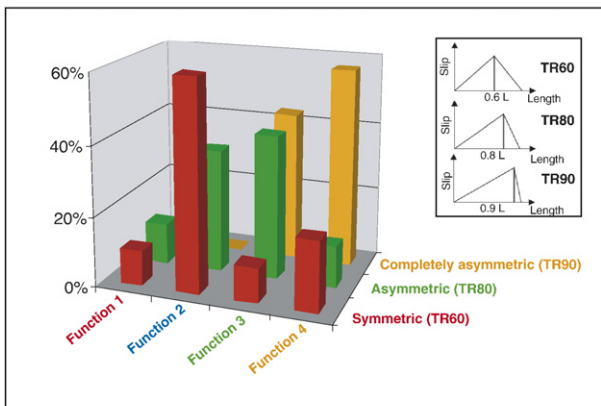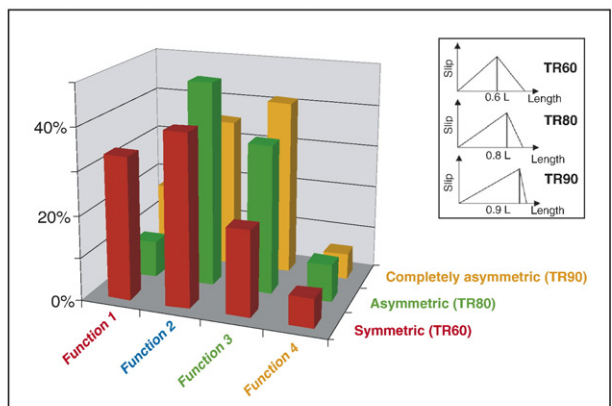

Fig. 4. Facing the segmentation scenario with independent data. (a) Number of broken segments as a function of proximity with optimal functions 1 to 4; the number of broken segments is observed to increase as one goes from function 1 to 4. (b) Asymmetry of surface slip profiles (from Table 2; inset recalls the 3 classes of asymmetry depicted by Manighetti et al., 2005) as a function of proximity with optimal functions 1 to 4; asymmetry is observed to increase as one goes from function 1 to 4. (c) Asymmetry of along-strike slip profiles at depth (from Table 3; inset as in b) as a function of proximity with optimal functions 1 to 4; asymmetry is observed to increase as one goes from function 1 to 4. (d) Structural maturity of broken geological faults (from Table 1) as a function of proximity with optimal functions 1 to 4; fault maturity is observed to increase as one goes from function 1 to 4.
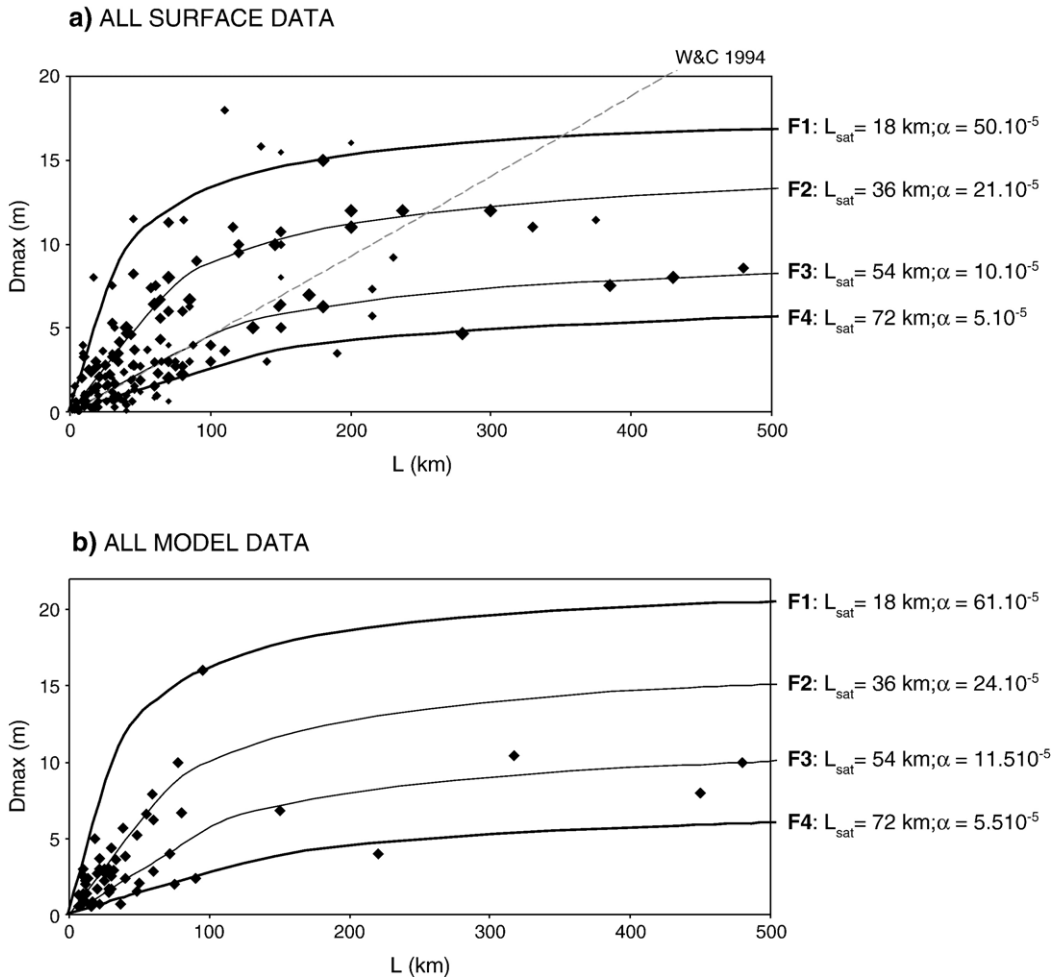
Fig. 5. Modeling the slip-length data. (a) Surface D_{max}–L data (from Table 2). (b) D_{max}–L data inferred at depth (from Table 3). Each global data set is shown with the theoretical functions deduced from the multi-segment rupture model. The regression of Wells and Coppersmith [19] is shown in A for comparison. Apparent stress drops vary from ~9 to 1 MPa as one goes from function 1 to 4 (in b). Yet, actual stress drop on individual crack-like segments only vary from ~9 to 3.5 MPa.

when several segments have been broken; in that later case, the segment with higher slip occupies approximately a third of the total rupture length. Fig. 4b–c report the degrees of asymmetry of ~90 earthquake slip profiles as defined by [21], measured at surface (Fig. 4b) or inferred at depth from inversion models (Fig. 4c). The data are presented with respect to the four optimal functions defined before. Overall, symmetric slip profiles are found for earthquakes pertaining to the data subsets best fitted by the optimal functions 1 or 2, while more asymmetric profiles are found for earthquakes pertaining to the data subsets best fitted by the optimal functions 3 to 4.

We have proposed that the strength of the large-scale inter-segment barriers depends on the structural maturity of the faults to which segments belong, with such

barriers being 'stronger' on immature faults, and 'weaker' on mature faults. Fig. 4d faces the structural maturity (as defined in Table 1) of the faults broken in 140 earthquakes, with the four optimal functions established from surface data. It confirms that overall, earthquakes occurring on immature faults pertain to groups 1 or 2, whereas earthquakes occurring on most mature faults pertain to groups 3 or 4.

6. Discussion and conclusions

Different pieces of evidence thus converge to suggest that the scenario proposed in Fig. 3 represents a valuable basis to interpret the earthquake D–L relationships. An earthquake would break a variable, yet limited number of major segments (or major 'asperities') along a fault,

depending on whether or not the breakage of the very first segment is 'energetic' enough to overcome the strength of the first encountered major inter-segment barrier, and trigger the rupture of the neighboring major segment(s). That capability of breaking inter-segment barriers would depend on the fault structural maturity; mature faults would be more prone to break in cascading events for their inter-segment barriers are quite narrow and smoothed, whereas more immature faults would more likely break in a single or double event for their inter-segment zones represent much stronger barriers to rupture propagation. The variability in displacement-length earthquake data would result from that multiple event rupturing process. Earthquakes breaking a single segment would behave as a single elastic crack with slip starting to saturate at $L = 2W_{seism}$, while earthquakes breaking several segments would behave as a juxtaposition of several cracks. As a consequence, the minimum rupture size at which slip starts saturating is different from one earthquake to the other, yet in the form $L_{sat} = n*(2W_{seism})$ with n the number of broken segments when those are assumed to be similar in length. Intermediate situations with segments of different lengths are likely to exist and result in the scatter of the data points in each subset (in addition to stress drop variability). Yet, it is noteworthy that a model with L_{sat} being multiple of the seismogenic thickness is actually most required by the data. Fig. 5 faces the available D_{max}–L data (surface: Fig. 5a; depth: Fig. 5b) to that theoretical model (defined for $W_{seism} = 18$ km). The adjustment is satisfying: the standard deviation of the residuals $\log(D_{obs})$–$\log(D_{predicted})$ calculated as in [19] is only 0.18. The stress drop variations that are suggested by the α variations are not as large as it seems when neglecting segmentation. Indeed, for a data subset corresponding to a n-segment rupture, the stress drop on each segment is $\Delta\sigma = n*\mu*(\alpha/2)$. The inferred stress drops are actually about the same on all broken segments, on the order of 3.5–9 MPa (calculated from inversion model data which are more characteristic of the ruptures at depth; Fig. 5b). The few MPa difference that is still observed obviously depends on fault structural maturity (Fig. 4d); segments on mature, hence weakened faults break in lower stress drop-earthquakes than segments on immature faults, as has been suggested before e.g., [22,29,37]. Note that we verified that this variation in apparent stress drop is not related with the effect of the finite size of the barriers between ruptured segments. Whatever that size (in a realistic range), a change in stress drop is required. The data suggest stress drops ranging from ~9 MPa for single segment-events on immature faults, to ~3.5 MPa for 4 segment-events on mature faults (Fig. 5b). We thus broaden the conclusions of Cao and Aki

(1986) and Anderson et al. (1996), stating that fault structural maturity is a major factor, if not the most important, that governs the stress drop of earthquakes, hence the amplitude of ground motions. Careful geological analyses of long-term faults should thus be included in any seismic hazard study. Fig. 5 shows that the maximum length of earthquakes is ~200 km for group 1, ~400 km for group 2, ~500 km for group 3, suggesting that major segments along worldwide faults are ~200 km-long. Together with the observation that stress-drop and segmentation are related, this explains why D_{max} tends to decrease with total length for large events as pointed out by [30].

Our reappraisal of displacement-length earthquake data has important implications on seismic hazard assessment. First, depending on their structural maturity, faults of similar length may produce significantly different amounts of slip; mature faults obviously break in long ruptures with low slip amplitudes (<4–7 m). By contrast, more immature faults break in shorter, yet more 'energetic' ruptures, on which slip as high as 15 m may be expected.

On the other hand, when one calculates the ratio between maximum slip measured at surface and maximum slip inferred at depth, that one finds that surface slip generally is only a fraction of actual slip at depth, averaging 85% for most large strike–slip ruptures ($M \geq 6.5$), 40% for small (~$6 \leq M < 6.5$) strike–slip, reverse and normal earthquakes, and even less than 10% for a few other cases (Fig. G, supporting online material). This suggests that surface measurements of slip cannot be used to calculate an earthquake magnitude unless they are 'corrected' by a certain factor.

Finally, our refined D–L earthquake 'scaling laws' are more accurate than those available (see in Fig. 5a a comparison with regression from Wells and Copper-smith, 1994; later referred to as W&C). We have calculated the standard deviation of the residuals $\log(D_{obs})$–$\log(D_{predicted})$ for our data set, using the W&C empirical relation $\log(D_{predicted}) = -1.38 + 1.02 \log(L)$. The standard deviation that we obtain is equal to 0.41, a value similar to the one obtained in the original paper of W&C from a smaller data set. Table 4 (supporting online material) indicates however that the residuals obtained with the W&C relation show a clear bias with earthquake size; the W&C model overestimates slip amplitudes for earthquakes with lengths greater than 200 km (see also Fig. 5a). To further compare our regressions with that of W&C, we have also calculated the residuals that would arise from fitting our entire data set with one single optimal S&S01 relation (that is found to have $W = 54.7$ km and $\alpha = 12.4 \ 10^{-5}$). The

variance is similar to the one obtained when using the W&C relation ($\sigma = 0.41$), but the residuals do not exhibit any bias with earthquake size. The residuals also approximately follow a log-normal distribution (Fig. H, supporting online material).

The standard deviation of the residuals obtained when using our best-fitting model with four curves is 0.18 when the entire data set is considered. For the best constrained Asian data set whose modeling requires only three curves, the standard deviation keeps as low (0.17). We checked that this decrease in standard deviation is not an 'artefact' due to the introduction of a too large number of parameters (over-fitting). This was done by computing the Akaike Information Criterion AIC; [43]. This criterion determines the balance between the model improvement and the number of free parameters that contribute to that improvement (increasing the number of free parameters always improves the fit). We computed the AIC for models with n curves and verified that that criterion is decreasing continuously with n, for n between 1 and 4. This test shows that our 4 curve-model significantly improves the residuals without over-fitting. This confirms the potential interest of modelling earthquake slip-length data with a multiple event-model of the form we propose.

In hazard studies where a critical issue is to reduce the uncertainties on seismic hazard assessment e.g. [44], our study may thus have some impact since it produces residues that are twice lower than those associated with available D–L regressions [19]. Our predictive $D_{max}-L$ functions could be used as distinct branches of a logic tree e.g., [45], each with an reduced aleatory variability compared to classical models. Weight assigned to each branch would depend on fault structural maturity (epistemic uncertainty). We are now in the process of refining the 'maturity criteria', so that more accurate functions may be established between earthquake slip and length, and fault structural maturity.

Acknowledgements

Appendix A. Supplementary data

Supplementary data associated with this article can be found, in the online version, at doi:10.1016/j.epsl.2006.11.004.

References

[1] K. Aki, Tectonophysics 13 (1972) 423.
[2] H. Kanamori, D.L. Anderson, Bull. Seismol. Soc. Am. 65 (1975) 1073.
[3] J.N. Brune, Seismic Risk and Engineering Decisions, 1976, p. 140.
[4] R. Madariaga, Bull. Seismol. Soc. Am. 66 (1976) 636.
[5] H. Kanamori, E.E. Brodsky, Rep. Prog. Phys. 67 (2004) 1429.
[6] C. Scholz, Bull. Seismol. Soc. Am. 72 (1982) 1.
[7] B. Romanowicz, Geophys. Res. Lett. 19 (1992) 481.
[8] B. Romanowicz, J. Rundle, Bull. Seismol. Soc. Am. 83 (1993) 1294.
[9] C. Scholz, Bull. Seismol. Soc. Am. 84 (1994) 215.
[10] C. Scholz, Bull. Seismol. Soc. Am. 84 (1994) 1677.
[11] B. Romanowicz, Bull. Seismol. Soc. Am. 84 (1994) 1675.
[12] P. Bodin, J.N. Brune, Bull. Seismol. Soc. Am. 86 (1996) 1292.
[13] J.H. Wang, S.S. Ou, Bull. Seismol. Soc. Am. 88 (1998) 758.
[14] T.C. Hanks, W.H. Bakun, Bull. Seismol. Soc. Am. 92 (2002) 1841.
[15] P.M. Mai, G.C. Beroza, Bull. Seismol. Soc. Am. 90 (2000) 604.
[16] B.E. Shaw, C.H. Scholz, Geophys. Res. Lett. 28 (2001) 2991.
[17] B. Romanowicz, L.J. Ruff, Geophys. Res. Lett. 29 (2002) 12.
[18] C. Scholz, C.A. Aviles, S.G. Wesnousky, Bull. Seismol. Soc. Am. 76 (1986) 65.
[19] D.L. Wells, K.J. Coppersmith, Bull. Seismol. Soc. Am. 84 (1994) 974.
[20] D.J. Dowrick, D.A. Rhoades, Bull. Seismol. Soc. Am. 94 (2004) 776.
[21] I. Manighetti, M. Campillo, C. Sammis, M. Mai, G. King, J. Geophys. Res. 110 (2005) B05302.
[22] T. Cao, K. Aki, Pure Appl. Geophys. 124 (1986) 515.
[23] J.G. Anderson, S.G. Wesnousky, M.W. Stirling, Bull. Seismol. Soc. Am. 86 (1996) 683.
[24] C. Marone, Annu. Rev. Earth Planet. Sci. 26 (1998) 643.
[25] S.A. Miller, Geophys. Res. Lett. 29 (2002), doi:10.1029/2001GL014181.
[26] M. Stirling, S.G. Wesnousky, K. Shimazaki, Geophys. J. Int. 124 (1996) 833.
[27] I. Manighetti, G.C.P. King, Y. Gaudemer, C. Scholz, C. Doubre, J. Geophys. Res. 106 (2001) 13667.
[28] Y. Ben-Zion, C.G. Sammis, Pure Appl. Geophys. 160 (2003) 677.
[29] K. Otsuki, T. Dilov, J. Geophys. Res. 110 (2005), doi:10.1029/2004JB003359.
[30] J. Liu-Zeng, T. Heaton, C. DiCaprio, Geophys. J. Int. 162 (2005) 841.
[31] D.P. Schwartz, K.J. Coppersmith, J. Geophys. Res. 89 (1984) 5681.
[32] L.J. An, C.G. Sammis, Tectonophysics 253 (1996) 247.
[33] B. Trudgill, J. Cartwright, GSA Bull. 106 (1994) 1143.
[34] J.J. Walsh, J. Watterson, W.R. Bailey, C. Childs, J. Struct. Geol. 21 (1999) 1019.
[35] M.J. Young, R.L. Gawthorpe, S. Hardy, J. Struct. Geol. 23 (2003) 1933.
[36] N.J. Richardson, J.R. Underhill, G. Lewis, Basin Res. 17 (2005) 203.
[37] S.G. Wesnousky, Nature 335 (1988) 340.
[38] K. Aki, J. Geophys. Res. 84 (1979) 6140.
[39] G. King, J. Nabelek, Science 228 (1985) 984.
[40] R.H. Sibson, Nature 316 (1985) 248.
[41] R.A. Harris, S.M. Day, J. Geophys. Res. 98 (1993) 4461.
[42] R.A. Harris, S.M. Day, Geophys. Res. Lett. 26 (1999) 2089.
[43] H. Akaike, IEEE Trans. Automat. Control 19 (1974) 716–723.
[44] F. Scherbaum, J. Bommer, H. Bungum, F. Cotton, N.A. Abrahamson, Bull. Seismol. Soc. Am. 95 (2005) 1575.
[45] J. Bommer, F. Scherbaum, H. Bungum, F. Cotton, F. Sabetta, N.A. Abrahamson, Bull. Seismol. Soc Am. 95 (2005) 377.